JOURNAL OF SOLID STATE CHEMISTRY **128,** 247–250 (1997)
ARTICLE NO. SC967199

On Characterization of Barium Rare-Earth Antimonates: Ordered Perovskites Suitable as Substrates for Superconducting Films

J. A. Alonso,* C. Cascales,* P. García Casado,† and I. Rasines*,[1]

*Instituto de Ciencia de Materiales, CSIC, Cantoblanco, 28049 Madrid, Spain; and †Facultad de Ciencias, Universidad de Navarra, 31080 Pamplona, Spain

Received July 11, 1996; accepted October 17, 1996

The crystal structure of the ordered perovskites $Ba_2(RSb)O_6$ (R = Y, Ho) is refined from neutron powder diffraction data in the space group $Fm\bar{3}m$ (No. 225), $Z = 4$, with Ba at 8(*c*), R at 4(*b*), Sb at 4(*a*), oxygen at 24(*e*), oxygen positional parameter $x = 0.2636(2)$ for R = Y and Ho, and unit cell dimensions of a/Å = 8.4240(3) and 8.4170(2) for R = Y and Ho, respectively. Bond-valence analysis explains how the highly covalent Sb–O bonds determine the overall structure of these perovskites in which R–O and Ba–O bonds are under compressive and tensile stresses, respectively. The magnetic susceptibility of $Ba_2(HoSb)O_6$ has been measured in the temperature range 2–350 K. From an *a priori* estimation of the crystal-field parameters corresponding to the point site symmetry of the rare-earth, O_h, and using the wavefunctions associated with the energy levels obtained, the paramagnetic susceptibility and its evolution vs temperature is simulated according to the van Vleck formalism. The observed deviation from the Curie–Weiss behavior at low temperature, very well reproduced, reflects the splitting of the ground state of this cation under the influence of the crystal field. © 1997 Academic Press

I. INTRODUCTION

The $Ba_2(RSb)O_6$ (R = rare earth) perovskites were known 30 years ago when Blasse established (1) that the Gd compound is cubic, $a = 8.44$ Å, and shows X-ray diffraction reflections characteristic of 1 : 1 order on the sublattice of the Gd and Sb cations. Later some of the present authors characterized (2, 3) nine perovskites of this family by X-ray powder diffraction, but they were not able to determine the oxygen positional parameter from X-ray diffraction data. These compounds were recently (4) shown to be suitable as substrates for $YBa_2Cu_3O_{7-\delta}$ thin films. As one promising application of high T_c superconducting thin films is the field of passive microwave devices including filters, resonators, delay and transmission lines, and antenna arrays, it seems recommendable to characterize more completely these possible substrates. This is the aim of this article.

II. EXPERIMENTAL DETAILS

Preparation. Polycrystalline samples of $Ba_2(RSb)O_6$ (R = Y, Ho) were prepared from mixtures of analytical grade BaO_2, R_2O_3, and Sb_2O_3 of molar ratios $Ba : R : Sb = 2 : 1 : 1.2$, which were heated in air at 800, 1000, 1200 and 1300°C. After each thermal treatment that lasted 1 day, the products were quenched, ground, and characterized by X-ray powder diffraction.

Neutron powder diffraction. The neutron powder diffraction diagrams of $Ba_2(RSb)O6$ (R = Y, Ho) were collected at room temperature in the multidetector DN5 diffractometer at the Siloé reactor of the Centre d'Etudes Nucléaires, Grenoble. A wavelength of 1.345 Å was selected from a Cu monochromator. The 800 detectors covered a 2θ range of 80°, from $2\theta_i = 12°$. The counting time for each diagram was about 4 h, using 10 g of sample contained in a vanadium can. The neutron diffraction patterns were analyzed by the Rietveld (5) method, using the FULLPROF program (6). Details of the refinement procedure are given elsewhere (7). The coherent scattering lengths for Ba, Y, Ho, Sb, and O were, respectively, 5.07, 7.75, 8.01, 5.57, and 5.805 fm.

Crystal-field levels and magnetic susceptibility calculation. The method used for calculating the energy levels and magnetic properties of the $Ho^{3+} + 4f^{10}$ configuration in its crystalline environment is based on the central-field approximation. The total Hamiltonian consists of two parts

$$H = H_{FI} + H_{CF},$$

where H_{FI} is the free-ion part, which includes the spherically symmetric one-electron term of the Hamiltonian, the electrostatic repulsion between equivalent f electrons, the spin–orbit interaction, and terms accounting for higher-order

[1] To whom correspondence should be addressed.

0022-4596/97 $25.00

corrections (8). Free-ion parameters for the $4f^{10}$ configuration of Ho^{3+} in $Ba_2(HoSb)O_6$ are assumed to be those reported by Carnall (8). H_{CF} is the crystal-field term, which takes into account the effect of the electrostatic interaction arising from the surrounding ions on the *f* electrons. In the presence of a crystalline electric field the degeneracy of each state of the free ion will be lifted according to the site symmetry of the rare-earth ion in the crystal lattice. Following Wybourne's formalism, the crystal-field Hamiltonian is expressed as a sum of products of spherical harmonics and crystal-field parameters (cfps):

$$H_{cf} = \sum_{k,q} (B_q^k [C_q^k + (-1)^q C_{-q}^k] + iS_q^k [C_q^k - (-1)^q C_{-q}^k]).$$

The number of the nonzero B_q^k and S_q^k phenomenological cfps depends on the crystallographic point-site symmetry of the lanthanide ion. When the O_h symmetry was considered for Ho^{3+} in $Ba_2(HoSb)O_6$ the crystal potential involves four real parameters where B_0^4 and B_4^4 keep a cubic relationship. Among all reported *a priori* calculation models of the cfps, that is known as the *Simple Overlap Model* (SOM) (9) has been applied in this case because it has been tested on similar compounds and gives results (10, 11) close to those experimentally determined. Only the first coordination sphere around the rare-earth cation is retained; i.e., required crystallographic positions are restricted to the closest ligand positions.

The calculation of the magnetic susceptibility has been carried out from the consistent sets of wavefunctions and energy levels previously determined by diagonalizing the above mentioned Hamiltonian. This is done using the van Vleck formula (12)

$$\chi(i) = N\beta^2 \sum_a \left[\frac{\langle \Phi_a | H | \Phi_a \rangle^2}{kT} - 2 \sum_b \frac{\langle \Phi_a | H | \Phi_b \rangle \langle \Phi_b | H | \Phi_a \rangle}{E_a - E_b} \right] B_a$$

in which N is Avogadro's number, β the Bohr magneton, k the Boltzman constant, E and ϕ the nonperturbed eigenvalues and wavefunctions, respectively, described on the $|SLJM_J\rangle$ basis, and H the magnetic dipole operator $L + g_e S$, represented by a first rank tensor having three components which characterize the magnetic anisotropy. The sums runs over all thermally populated levels, according the Boltzmann population, $B_a = \exp(-E_a^{(0)}/kT)/\sum_a \exp(-E_a^{(0)}/kT)$. In that expression, the matrix elements are calculated using the Racah algebra rules.

Except for Eu^{3+} and to a less extent for Sm^{3+} compounds, the diagonal part, i.e., the temperature-dependent term of χ, is the most important contribution to the paramagnetic susceptibility. In fact it corresponds to the quantum expression of the Curie–Weiss law, $\chi = C/(T + \theta)$. The off-diagonal, temperature-independent terms in the formula, a result of the second-order perturbation, usually have small importance, except for the ground states with $J = 0$.

Calculations of the energy levels and paramagnetic susceptibility were performed by Fortran programs REEL and IMAGE (13).

Magnetic measurements. A *Quantum Design PPMS6000* magnetometer with an absolute resolution of 2.5×10^{-5} emu was used to perform the dc magnetic measurements from 350 to 2 K at 10 kOe. Diamagentic corrections (14) for magnetic susceptibilities were introduced.

III. RESULTS

The X-ray diffraction patterns of $Ba_2(RSb)O_6$, or $Ba(R_{1/2}Sb_{1/2})O_3$, were characteristic of cubic perovskites, showing very weak superstructure reflections that made it necessary to consider a doubled cubic unit cell, $2a_0 \times 2a_0 \times 2a_0$ ($a_0 \approx 4$ Å is the edge of the simple cubic ABO_3 perovskite). For R = Y, Ho, a = 8.4240(3) and 8.4170(2) Å, respectively. The cell parameter for R = Ho is equal to that previously (2) determined. In this superstructure R and Sb are 1:1 ordered in the *B*-cation sublattice, giving rise to a face-centered lattice. The superstructure reflections (111, 311, 331, ...) are associated with the R:Sb ordering and with the displacements of the oxygen atoms toward the smaller *B* cations, the Sb^{5+} cations. These are considerably smaller, 0.60 Å for sixfold coordination, that Y^{3+} or Ho^{3+}, whose ionic radii for the same coordination are 0.900 and 0.901 Å, respectively (15).

The same superstructure reflections were observed in the neutron diffraction diagrams. These reflections were strong

TABLE 1
Structural Parameters after the Refinement of Neutron Powder Diffraction Data for Ba(RSb)O_6 at 295 K

R	Y	Ho
a/Å	8.4240(3)	8.4170(2)
V/Å^3	597.80(9)	596.31(6)
M/g mol^{-1}	581.33	657.36
d_c/g cm^{-3}	6.46	6.64
x(O)	0.2636(2)	0.2636(2)
B(Ba)	0.51(4)	0.51(3)
B(R)	0.12(6)	0.10(7)
B(Sb)	0.53(10)	0.67(10)
B(O)	0.70(3)	0.76(2)
R_p	3.12	2.22
R_{wp}	4.39	2.94
R_I	2.42	2.07

Note. Space group $Fm\bar{3}m$ (No. 225), $Z = 4$. Ba atoms are at 8*c* (1/4, 1/4, 1/4) positions, R at 4*a* (0,0,0), Sb at 4*b* (1/2, 1/2, 1/2), and O at 24*e* (x, 0, 0). Isotropic B thermal factors are given in Å^2.

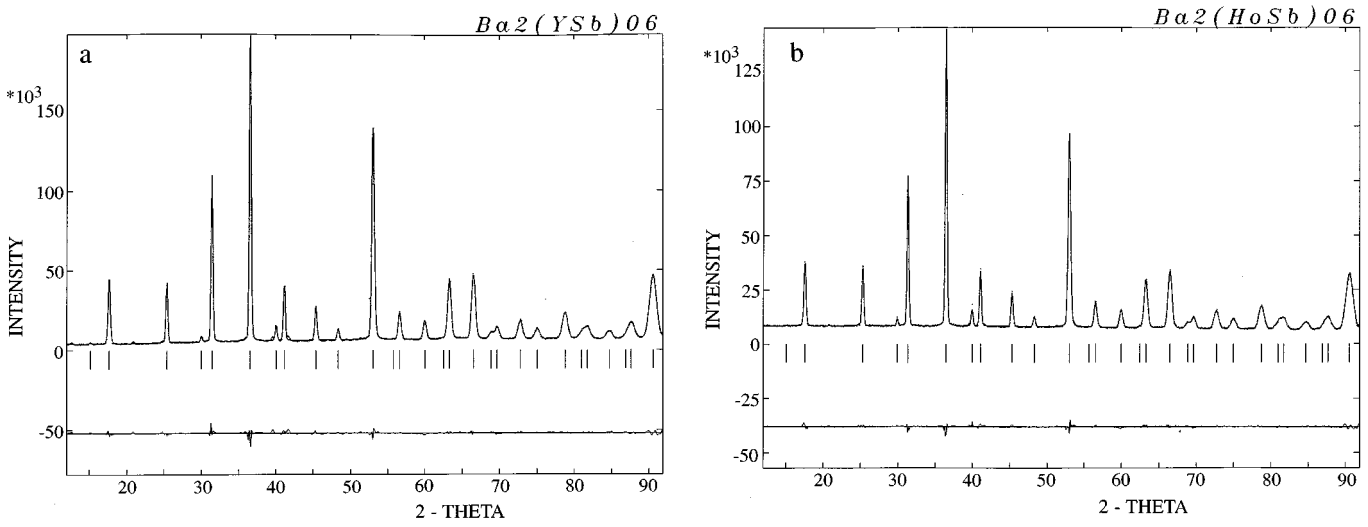

FIG. 1. Observed (crosses), calculated (solid line), and difference (bottom) neutron diffraction profiles for (a) $Ba_2(YSb)O_6$ and (b) $Ba_2(HoSb)O_6$ at 295 K. The tick marks indicate the positions of the allowed Bragg reflections.

enough to allow us to obtain information about the displacement of the oxygen atoms. Moreover, no additional superstructure reflections or splitting of the peaks were detected, excluding the presence of tilting of the BO_6 octahedra. The structure was refined in the $Fm3m$ space group, with the only variable structural parameter corresponding to the oxygen positions. The results of the refinement are summarized in Table 1. The goodness of fit is shown in Fig. 1. Table 2 contains a selected list of distances and angles, and a view of the structure is illustrated in Fig. 2 for $R = Y$.

In the crystal structure of $Ba_2(RSb)O_6$ both Sb^{5+} and R^{3+} cations are in a regular octahedral environment, the SbO_6 and RO_6 octahedra alternating along the three axes, as shown in Fig. 2. The Sb–O distances are very close in both compounds, 1.991(2) and 1.990(2) Å for the Y and Ho perovskites, respectively, and precisely compare with the sum of ionic radii for Sb^{5+} and O^{2-}, 2.00 Å, taking the radius of O^{2-} as 1.40 Å (4). The ionic approach is less successful if we consider the *R*–O distances: the observed *R*–O bond lengths are 2.221(2) and 2.219(2) Å for $R = Y$ and Ho, respectively, whereas the ionic radii sums take the relatively high values of 2.300 and 2.301 Å.

It is somewhat unusual to find a rare-earth cation occupying the *B* positions of a perovskite: given their relatively high size they are more often found in the *A* sublattice, e.g., in the well known $RFeO_3$ family. A bond valence analysis, after Brown's model (16, 17), can help give an idea of how *comfortable* a rare-earth cation is in the *B* sublattice of a perovskite. Table 3 lists the bond valence sums (BVS) corresponding to all the cations of the $Ba_2(RSb)O_6$ structures. Observe that the BVS for Sb is close to the expected value of 5+ (within about 5% of deviation). In contrast, BVS for both Y and Ho are remarkably above the expected valence of 3+. The opposite trend is observed for Ba, showing BVS values slightly lower than 2. According to that, rare-earth cations are strongly overbonded in the structure, this effect being balanced by the somewhat underbonded Ba cations. The small thermal *B* factors observed

TABLE 2
Interatomic Bond Distances (Å) for BaO_{12}, RO_6 and SbO_6 Coordination Polyhedra in $Ba(RSb)O_6$ Perovskites

R		Y	Ho
Ba–O	(×12)	2.981(1)	2.978(1)
R–O	(×6)	2.221(2)	2.219(2)
Sb–O	(×6)	1.991(2)	1.990(2)

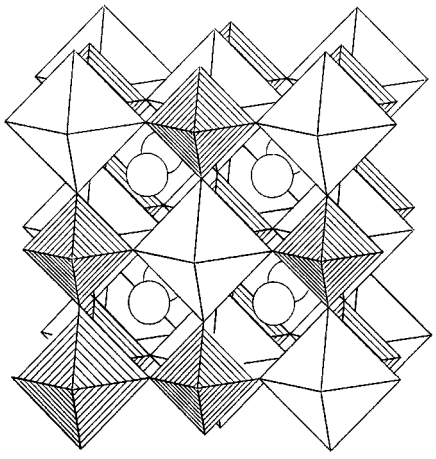

FIG. 2. View of the $Ba_2(YSb)O_6$ structure. Open octahedra correspond to Y atoms and hatched octahedra to Sb atoms. Both kinds of octahedra alternate according to a 1 : 1 arrangement. Ba atoms (open circles) are in the voids formed by the octahedra.

TABLE 3
Bond Valence Sums (BVS)[a] and Deviations (%) with Respect to the Expected Valence for Ba, *R*, and Sb within the Coordination Polyhedra to Oxygen in Ba(*R*Sb)O_6

R	Y		Ho	
	BVS	dev(%)	BVS	dev(%)
Ba	1.856	7.18	1.869	6.56
R	3.435	14.49	3.534	17.82
Sb	5.247	4.94	5.274	5.49

[a] BVS is the sum of the individual bond valences (s_i) for Ba–O, R–O, and Sb–O bonds. Bond valences are calculated[10] as $s_i = \exp[(r_0 - r_i)/B]$; $B = 0.37$, $r_0 = 2.290$ for the Ba^{2+}–O^{2-} pair, $r_0 = 2.014$, 2.023 for the (Y^{3+}, Ho^{3+})–O^{2-} pairs, and $r_0 = 1.942$ for the Sb^{5+}–O^{2-} pair. Individual Ba–O, R–O, and Sb–O distances (r_i) are taken from Table 2.

for both Y and Ho (Table 1) also support the overbonded character of the *R*–O chemical bonds. In other words, *R*–O bonds are under compressive stresses whereas Ba–O bonds are under tensile stresses. This result suggests that the highly covalent Sb–O bonds determine the overall structure of these perovskites, in which oxygen atoms are placed in such a way that SbO_6 octahedra have optimized Sb–O bond lengths. *R* and Ba cations are linked to oxygens through more ionic, flexible interactions that enable the stability of the crystal structure in spite of the stresses related to the large size of the rare-earth cations.

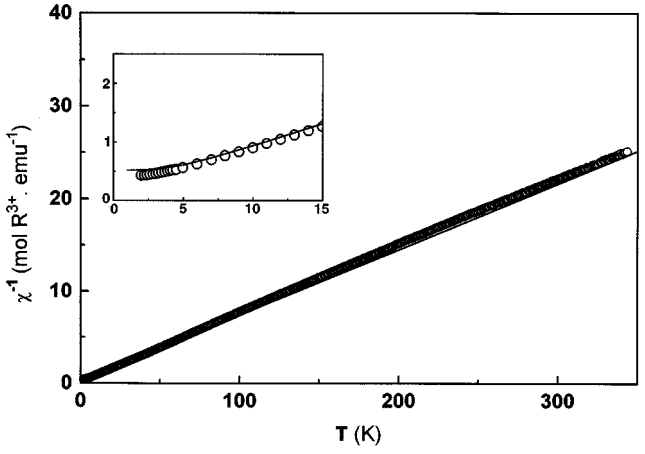

FIG. 3. Comparison between experimental (circles) and calculated (solid line) reciprocal paramagnetic susceptibilities for $Ba_2(HoSb)O_6$. Inset represents the enlargement of the low temperature data.

The evolution of the reciprocal paramagnetic susceptibility χ^{-1} with temperature for $Ba_2(HoSb)O_6$ is shown in Fig. 3. Above 10 K this compound presents Curie–Weiss behavior ($r = 0.9998$), $\theta_c = -5.6$ K. Deviation from linearity at low temperatures is attributed to the splitting of the ground term $^5I_8$ of Ho^{3+} under the influence of its surrounding crystal field. The superimposed curve corresponds to the simulation of χ^{-1} through estimated cfps (cm^{-1}), $B_0^4 = 731$, $B_4^4 = 437$, $B_0^6 = 148$, $B_4^6 = -277$. Very good agreement is found between both curves, with effective magnetic moments, μ_B, of 10.44(4) and 10.50(6) for experimental and calculated curves, respectively, in the 350–100 K region. Thus, the standard crystal-field treatment of this trivalent lanthanide cation is shown to explain the magnetic susceptibility of this compound, for which no magnetic interactions among the rare-earth ions have been detected.

ACKNOWLEDGMENTS

This work was supported by the CICyT of Spain, under Project PB94-0046. We thank Dr. J. L. Martínez for performing the magnetic measurements. We also thank Dr. P. Porcher for letting us use his unpublished programs.

REFERENCES

1. G. Blasse, *J. Inorg. Nucl. Chem.* **27,** 993 (1965).
2. P. García Casado, A. Mendiola, and I. Rasines, *Z. Anorg. Allg. Chem.* **510,** 194 (1984).
3. Powder Diffraction File, Cards 371111–371113. International Centre for Diffraction Data, Newtown Square, PA.
4. J. Kurian, J. Koshy, P. R. S. Wariar, Y. P. Yadava, and A. D. Damodaran, *J. Solid State Chem.* **116,** 193 (1995).
5. H. M. Rietveld, *J. Appl. Crystallogr.* **2,** 65 (1969).
6. J. Rodríguez-Carvajal, *Physica B* **192,** 55 (1993).
7. J. A. Alonso and M. J. Martínez-Lope, *J. Chem. Soc. Dalton Trans.* (1995) 2819.
8. W. T. Carnall, G. L. Goodman, K. Rajnak, and R. S. Rana, *J. Chem. Phys.* **90,** 3443 (1989).
9. L. M. Malta, *Chem. Phys. Lett.* **88,** 353 (1982).
10. C. Cascales, P. Porcher, and R. Sáez-Puche, *J. Phys.: Cond. Matter.* **8,** 6413 (1996).
11. C. Cascales, P. Porcher, and R. Sáez-Puche, *J. Alloys Compds.* in press.
12. J. H. van Vleck, *J. Appl. Phys.* **39,** 365 (1968).
13. P. Porcher, Fortran routines REEL and IMAGE for simulation of d^n and f^n configurations involving real and complex crystal-field parameters, unpublished, 1989.
14. L. N. Mulay, "Magnetic Susceptibility," p. 1782. Wiley, New York, 1963.
15. R. D. Shannon, *Acta Crystallogr., Sect. A* **32,** 751 (1976)
16. I. D. Brown, *in* "Structure and Bonding in Crystals" (M. O'Keefe and A. Navrotsky, Eds.), Vol. 2, pp. 1–30. Academic Press, New York, 1981.
17. N. E. Brese and M. O'Keefe, *Acta Crystallogr., Sect. B* **47,** 192 (1991).